A Dual-Mode Circular Antenna Array for Indoor Communication

Shen-Yun Wang[1,*], Meng-Ting Yang[1], Qing Zhang[2], Ling-Bing Kong[3], and Wen Geyi[1]

[1]*Research Center of Applied Electromagnetics, Nanjing University of Information Science and Technology, Nanjing 210044, China*
[2]*Shanghai Academy of Spacecraft Technology Beijing R&D Center, Beijing 100041, China*
[3]*Shanghai Aerospace Electronics Technology Institute, Shanghai 201109, China*

ABSTRACT: A circular antenna array with omnidirectional mode and 360° continuously directional beam-scanning mode operating in 5G indoor communication band is reported. The proposed circular antenna array is composed of 16 subarray elements, and each element consists of two back-to-back E-shaped patch antennas with a differential feeding network. The beam-scanning mode is achieved by controlling the exciting amplitudes and phases of consisting subarray elements, which is optimized by using the extended method of maximum power transmission efficiency, so as to guarantee the maximum possible gain value. The operating frequency of the circular array covers 3.3–3.6 GHz. The omnidirectional gain is about 4.7 dBi, while the directive gain reaches 16 dBi with 360° continuously beam-scanning capability and very slight gain fluctuation in the azimuth plane. The comparison with other state-of-the-art designs shows that the proposed circular array has both higher directional and omnidirectional gain values.

1. INTRODUCTION

With the growing data traffic of mobile communication, indoor base station has become an indispensable equipment because of the increasing demands on the quality and capacity of 5G system. Many potential solutions have been proposed to increase the capacity for wireless communication system, such as taking millimeter wave (mmWave) as the carrier frequencies, using the massive multiple-input-multiple-output (MIMO) technique [1]. Although mmWave systems have advantages in terms of high data rates, highly directive antenna with smaller footprints, there exist many inherent challenges, such as high path loss and blockages of human body or other objects in the indoor environment. Hence, the sub-6 GHz wave still draws increased attention in the 5G indoor communication [2–5].

In the early stages, omnidirectional antennas have been proposed for indoor base station application due to the 360° full coverage [6–8]. Recently, omnidirectional antennas with dual polarizations have been reported to counteract the multipath fading and polarization mismatch [9, 10]. However, omnidirectional radiation usually results in severe multi-path interferences due to the reflections from the ground and walls in the indoor environment. On the contrary, directional antennas with beam-scanning can improve the quality of the wireless link and reject interference as they can enable beam scanning or switching to the targeted user ends (UEs), while suppressing unwanted signals [11]. Hence, these types of antennas are identified as an attractive solution for 5G communication networks in sub-6 GHz band.

To realize a 360° signal coverage, circle-phased antenna arrays [12–20] and electronically steerable parasitic array radia-

tors (ESPARs) are commonly employed [21–24]. For ESPARs, one monopole or dipole is usually selected as the driven element, while several parasitic elements are introduced to adjust the antenna reactance to achieve the beam switching function. However, these types of antennas are less flexible as the directive radiation pattern is only reconfigurable among several states. For circular phased antenna arrays, the amplitude and phase of each individual element must be controlled to steer the beam in a specific direction. By modifying the exciting phases and amplitudes, a 360° continuously beam-scanning range in azimuth plane is achievable [25]. However, most circular antenna arrays with beam-scanning or -switching have achieved a small directive gain below 10 dBi [12–20]. This is mainly attributed to the fact that the radiator associated with the directional beam consists of either a single element or a small part of the elements of the circular array.

To get maximum possible directional gain of the designed circular antenna array, all the elements should be properly controlled. In fact, there are many beam synthesizing methods that have been proposed for circular and planar antenna arrays, such as least-squares method [26], differential evolution algorithm [27], evolutionary optimization algorithm [28], deep leaning technique [29], and linear programming approach [30]. Due to the assumption of some simplifications, such as identical element patterns and ignored manufacture tolerance, inconsistency happens between the theoretical predictions and full wave simulations and/or measurements.

In this paper, a circular antenna array that can work in omnidirectional mode and 360° continuously directional beam-scanning mode is designed. The novelties of this letter lie in both the higher omnidirectional and directive gain values of the circular array due to the proposed high-gain sub-array element using two back-to-back E-shaped patches, as well as 360° con-

tinuously beam-scanning performance in azimuthal plane with very slight gain fluctuation ($< 0.2\,\text{dB}$), so as to avoid gaps between the multiple beams, which results in a large area of signal coverage.

2. INDOOR BASE STATION ANTENNA ARRAY DESIGN

To realize omnidirectional signal coverage when the positions of UEs are unknown and directional beam once the positions of UEs are confirmed [31, 32], a circular antenna array is designed and fabricated.

2.1. Configuration of the Circular Antenna Array

At first, an elementary subarray element is designed, and its geometry is illustrated in Figure 1. It consists of two back-to-back E-shaped microstrip patches over a ground plane, where a single E-shaped patch has been demonstrated to work in a wide-band by introducing two slots on a rectangular patch [33]. The dielectric substrates of both the ground layer and E-shaped patch layer are Rogers 4350 with dielectric constant of 3.66, loss tangent of 0.003, and thickness of 1.524 mm. To generate a sum-pattern of the subarray element, a microstrip differential feed network is designed on the bottom side of the ground substrate to excite the two back-to-back E-shaped patches, as illustrated by the subarray through bottom view in Figure 1.
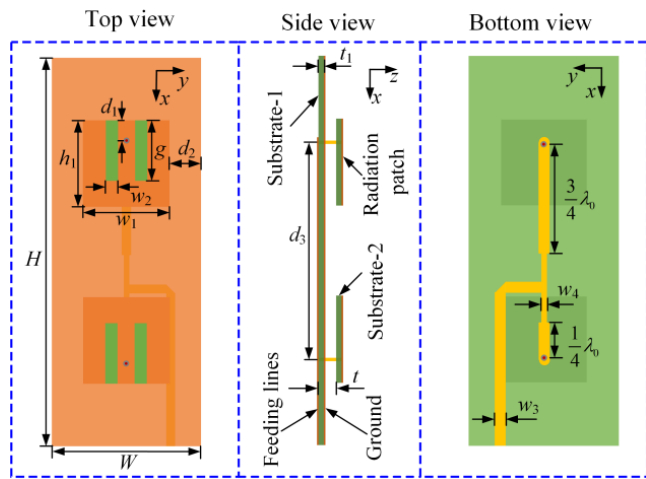

FIGURE 1. Top view, side view, bottom view of the sub-array element.

In this work, the antenna array is designed for 5G indoor communication covering a frequency band 3.3–3.6 GHz. Using the Ansys HFSS, the optimized geometrical parameters are listed in Table 1. The reflection coefficient ($|S_{11}|$) and port-to-port isolation ($|S_{21}|$) of the subarray element are plotted in Figure 2(a), where the $-10\,\text{dB}$ impedance matching bandwidth ranges from 3.1 to 4.2 GHz, which covers the 5G indoor communication band, and the isolation is below $-20\,\text{dB}$ in the simulation frequency band. The reflection and transmission coefficients of the microstrip differential feeding network are also simulated, which operates as an identical two-way power divider with $|S_{21}|$ and $|S_{31}|$ equal to $-3\,\text{dB}$ and $180°$ phase difference, as plotted in Figure 2(b).

TABLE 1. Geometrical parameters of the sub-array element.

Name	Value (mm)	Name	Value (mm)
W	52	g	21
H	136	d_3	76
w_1	30	t	6.476
h_1	30	d_2	11
w_2	4	w_3	3.2
d_1	8	w_4	1.6

Radiation patterns at 3.4 GHz of a single E-shaped patch and the subarray element are simulated, as plotted in Figures 3(a) and (b), respectively. It can be seen that the gain pattern of the single E-shaped patch is asymmetrical in *xoz*-plane due to the asymmetrical configuration along x-axis, as shown in Figure 3(a). Hence, two back-to-back E-shaped patches are introduced to obtain a symmetrical configuration along both x- and y-axes. As a result, a symmetrical pattern with high gain value is obtained, as shown in Figure 3(b).

Next, the circular antenna array is built with 16 subarray elements with diameter of 200 mm, and the simulated and fabricated antenna arrays are shown in Figures 4(a) and (b), respectively.

2.2. Beam-Scanning Approach

When all the subarray elements are identically excited, an omnidirectional radiation pattern is obtained to cover the UEs at any position in the azimuth plane. If the position of a UE is confirmed, a precise directional beam is needed to ensure a better received signal strength. In fact, in the design of any wireless communication system, the essential target is to maximize the power transmission efficiency (PTE) between the transmitter and receiver. For this reason, the maximum possible gain of the directional beam can be realized through the methodology of the extended method of maximum power transmission efficiency (EMMPTE) [34].

As illustrated in Figure 5, it is assumed that a UE is locatef at $P(r_p, \varphi_p)$ in the far-field zone, and there is a mapping position $P'(r_0, \varphi_p)$ on a far-field circle with respect to the circular antenna array, where r_0 is the specific radius of the circle. For the array is linearly polarized, we may let the electric field $\mathbf{E} = \mathbf{u}_z E$ with $\mathbf{u}_z$ being the unit vector along z-axis. To direct the radio signal to the UE direction, a specific performance index is newly introduced as

$$PTE = \frac{\frac{\varepsilon_0}{2}\,|E\,(P')|^2}{P_{in}} \qquad (1)$$

where the numerator is the total electric field energy density at the mapping position, and the denominator stands for the input power of the antenna array. When all the transmitting subarray elements are well matched, the total electrical field at the
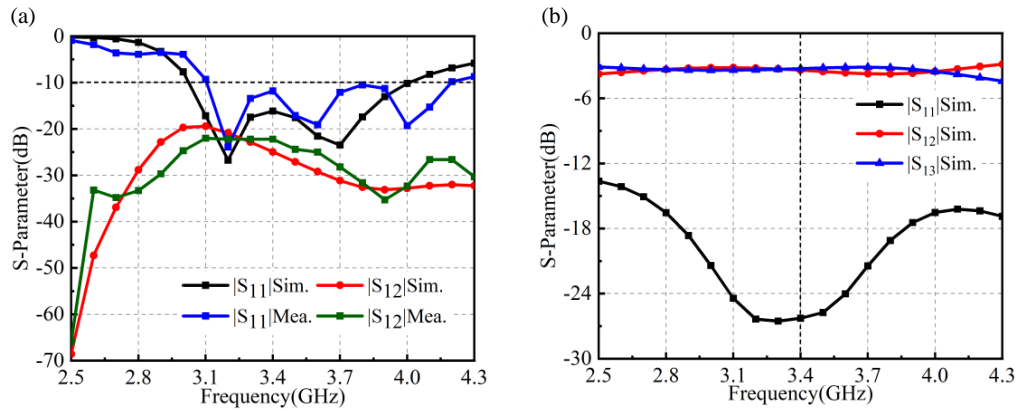
FIGURE 2. (a) Simulated and measured reflection and isolation of the sub-array antenna; (b) Simulated reflection and transmission coefficients of the feed network.
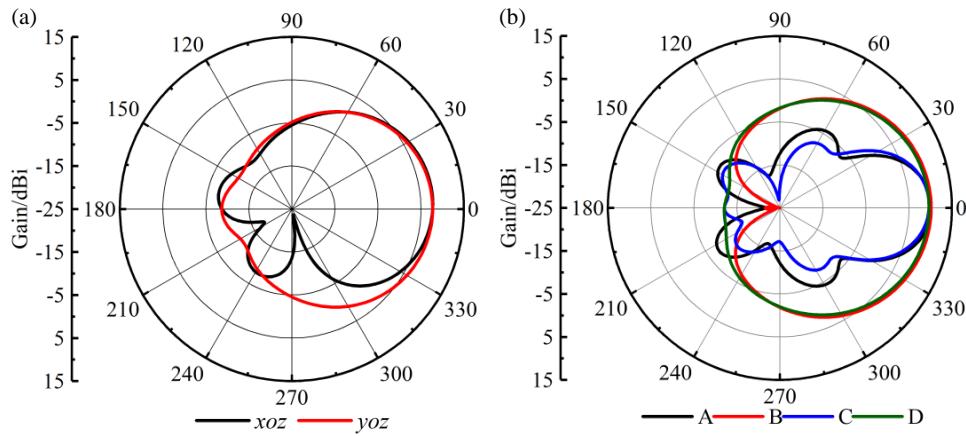
FIGURE 3. (a) Gain pattern of the single E-shaped patch in E-plane (xoz-plane) and H-plane (yoz-plane); (b) Gain pattern of sub-array (Line A and Line B are the patterns in xoz-plane and yoz-plane when the sub-array is fed by difference phases and identical amplitudes; Lines C and D are the patterns in xoz-plane and yoz-plane when the sub-array is fed by the difference feeding network).
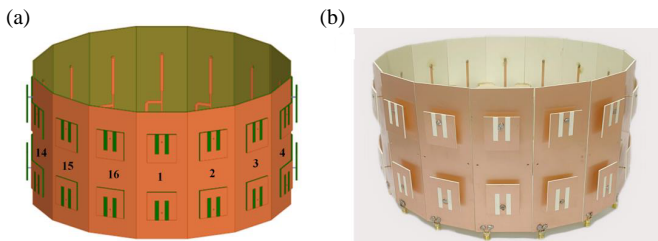
FIGURE 4. (a) Simulation model of the circular antenna array; (b) Photo of the fabricated circular antenna array.
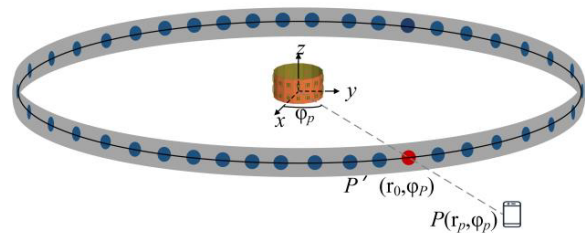
FIGURE 5. Wireless transmission system.

mapping position can be expressed as

$$E\left(\mathbf{r}_p\right) = \sum_{j=1}^{N} a_j E_j\left(P'\right) \qquad (2)$$

where N is the number of the sub-array elements, and $E_j(P')$ is the electrical field generated by the jth transmitting subarray element at the mapping position when it is excited by $a_j = 1$,

while the other subarray elements are terminated in their own characteristic impedances. Hence, the total electric fields at mapping position can be written as

$$E\left(P'\right) = [E_{rt}][a] \qquad (3)$$

where

$$[E_{rt}] = [E_1\left(P'\right), E_2\left(P'\right), \cdots, E_N\left(P'\right)],$$

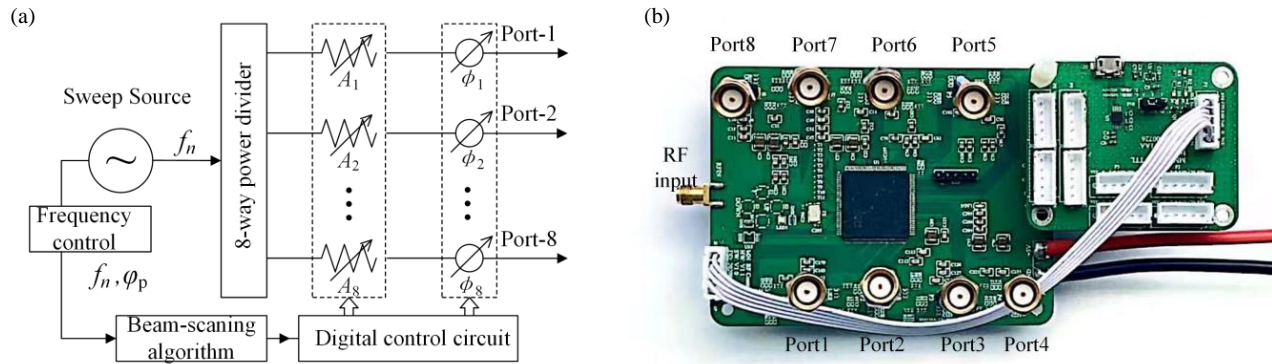$$[a] = [a_1, a_2, \cdots, a_N]^T,$$

(a)

(b)

FIGURE 6. Digital control feeding circuit. (a) Schematic; (b) Photo.

Making use of (2) and (3), the performance index (1) can be written as

$$PTE = \frac{\frac{\varepsilon_0}{2}\,|[E_{rt}][a]|^2}{\frac{1}{2}\,|[a]|^2} = \frac{\langle[A][a],\,[a]\rangle}{\langle[a],\,[a]\rangle} \tag{4}$$

where $[A] = \varepsilon_0[\bar{E}_{rt}]^T[E_{rt}]$ and $P_{in} = |[a]|^2/2$. It can be seen that the PTE is determined by the excitations $[a]$. By maximizing (4), an eigenvalue equation is obtained as

$$[A][a] = PTE \cdot [a]. \tag{5}$$

It can be solved by using QR decomposition method, and there is only one nontrivial eigenvalue that gives the maximum PTE. The eigenvector corresponding to the eigenvalue is the optimized distribution of excitations (ODEs) of the circular antenna array to generate the maximum possible gain in the UE direction. As the electrical fields of each sub-array element on the far-field circle are extracted in advance, the ODEs can be calculated by using (5) in real-time once the UE direction is confirmed.

2.3. Digital Controlled Feeding Circuit

When the ODEs are obtained using (5), a digital control feeding circuit is designed to excite the circular antenna array. A beam in any direction is generated by exciting the subarray elements around the beam axis, and an 8-channel digital-control RF feeding circuit is designed, which consist of RF source, digital-control circuit, 8-way power divider, 6-bit phase shifter with $5.625°$ ($360°/2^6$) phase resolution, 6-bit attenuator with maximum attenuation values of $31.5\,\text{dB}$ and $0.5\,\text{dB}$ ($31.5\,\text{dB}/2^6$) amplitude resolution in each RF feeding channel. The schematic and photo of the digital control RF feeding circuit are illustrated in Figures 6(a) and (b), respectively.

3. RESULTS AND DISCUSSIONS

The antenna system is set up with the fabricated circular antenna array, feeding circuit, connecting cables, and a laptop computer, as shown in Figure 7. The ODEs for different beam patterns are calculated on the laptop computer and transferred to the feeding circuit through a USB cable. Next, two working modes of the antenna system are demonstrated and tested in a microwave anechoic chamber.
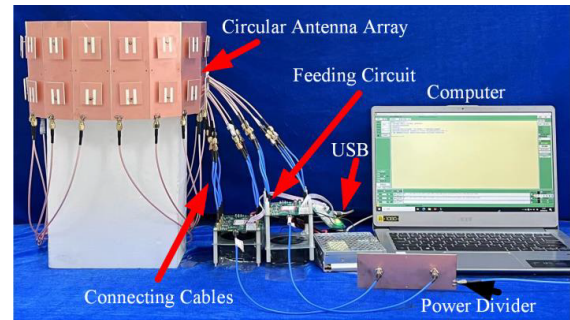

FIGURE 7. The setting up of the antenna system.

3.1. Omnidirectional Mode

When all the 16 subarray elements are excited in-phase with identical amplitude though two fixed 8-channel feeding networks, the circular antenna array operates in omnidirectional mode. The gain patterns in xoy-plane (H-plane) and xoz-plane (E-plane) are shown in Figures 8(a) and (b), respectively. It can be seen that the gain patterns are symmetrical with respect to z-axis, and the average simulated/measured gain is about $4.7\,\text{dBi}$ with very slight gain fluctuations ($< 0.2\,\text{dBi}$).

3.2. Directional Mode

Once the UE position is determined, the ODEs for directional beam can be timely calculated from (5). Due to the symmetry of the antenna configuration, the directional beam pointing to arbitrary UE direction is demonstrated in a $90°$ sector. The directional beams directed to $0°$, $15°$, $30°$, $45°$, $60°$, and $90°$ in the azimuth plane are shown in Figure 9, where the ODEs for $0°$ and $30°$ beam directions are listed in Table 2. It can be seen that the simulated and measured gain patterns agree well. The directional gain reaches $16\,\text{dBi}$, and it remains stable versus the azimuth angle. It is found from Table 2 that the subarray elements closer to the beam axis have larger amplitude values, while exciting amplitudes of the opposite 8 subarray elements are very small. Hence, they are not excited in the experiment.

3.3. Discussions

The directional beam is synthesized based on the extracted electrical fields of each subarray element, which contains the infor-
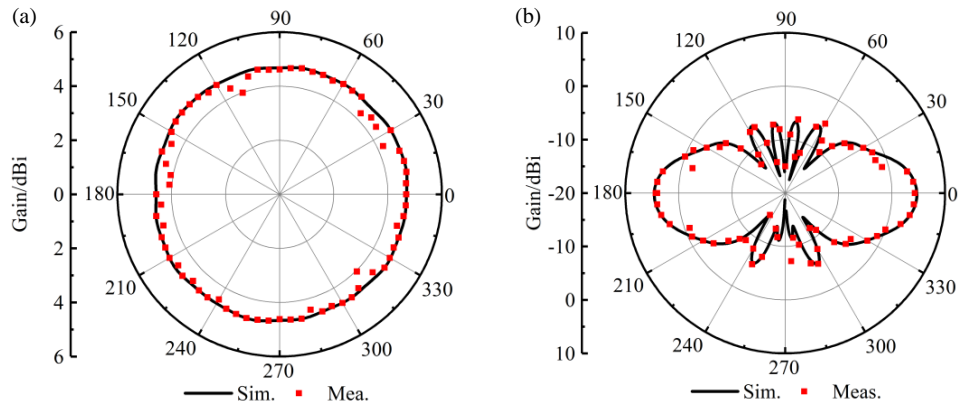
FIGURE 8. Simulation and measured radiation pattern in (a) *xoy*-plane (*H*-plane) and (b) *xoz*-plane (*E*-plane).
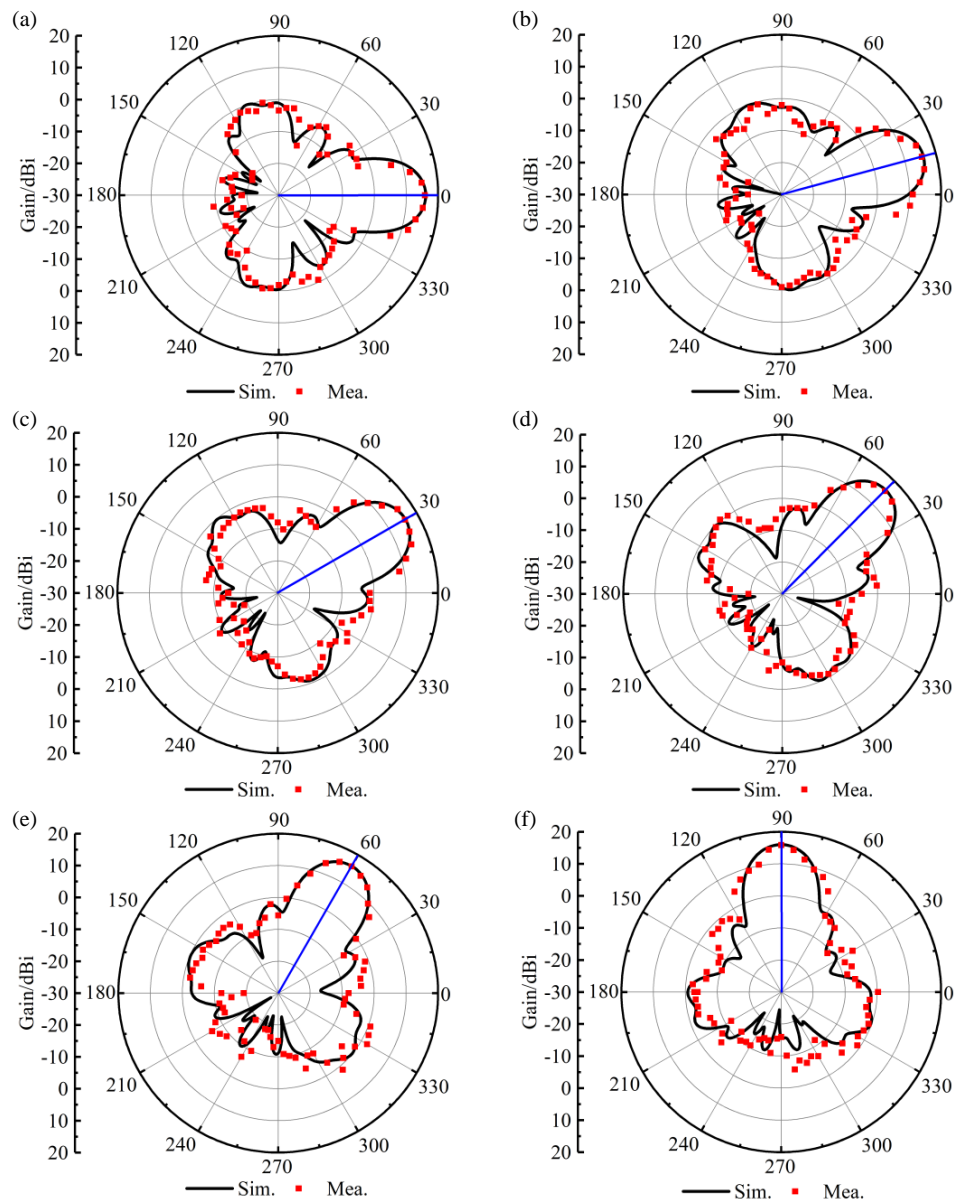

FIGURE 9. Simulated and measured gain patterns with beam directions at (a) 0°, (b) 15°, (c) 30°, (d) 45°, (e) 60°, (f) 90° in the azimuth plane.

TABLE 2. OEDs of the circular array for beam directions at 0° and 30°.

Port	0°	30°	Port	0°	30°
1	0.40∠82°	0.13∠171°	9	0∠0°	0∠0°
2	0.25∠135°	0.41∠89°	10	0∠0°	0∠0°
3	0.04∠ −95°	0.3∠106°	11	0∠0°	0∠0°
4	0∠0°	0.11∠ −147°	12	0∠0°	0∠0°
5	0∠0°	0.01∠21°	13	0∠0°	0∠0°
6	0∠0°	0∠0°	14	0.02∠88°	0∠0°
7	0∠0°	0∠0°	15	0.04∠ −97°	0.01∠151°
8	0∠0°	0∠0°	16	0.25∠135°	0.03∠ −40°

TABLE 3. Comparisons with other designs.

Ref. No.	Height × Diameter (λ_0)	BW	Beams	Omnidirectional gain (dBi)	Directional gain (dBi)
[11]	1.3 × 4	8.2%	12	-	9.2
[12]	0.51 × 0.39	10.8%	8	-	4.7
[17]	0.1 × 0.612	33.6%	3	-	7.13
[28]	0.28 × 0.9	12.4%	4	-1.8	6.0
[29]	0.4 × 0.32	18.8%	8	2.8	8.4
This paper	0.59 × 2.54	32%	Continuous	4.7	16

mation of mutual coupling between the elements and its install platform. As a result, both high-precision beam direction and maximum possible directional gain are guaranteed. The beam can be directed to any angle in the azimuth plane, resulting in a 360° continuously beam-scanning. The performance of the dual modes is compared with some other state-of-the-art designs, as summarized in Table 3. It is found that the proposed antenna has both higher directional and omnidirectional gain values, resulting in larger signal coverage area.

4. CONCLUSIONS

In this paper, a circular antenna array is designed and fabricated for the purpose of 5G indoor communication. It can operate in both omnidirectional mode and 360° continuously beam-scanning mode. Compared with the other state-of-the-art designs, the proposed circular antenna array is featured with both high omnidirectional and directional gain values and 360° continuous beam-scanning capability with very slight gain fluctuation in azimuth plane.

REFERENCES

[1] Yang, B., Z. Yu, Y. Dong, J. Zhou, and W. Hong, "Compact tapered slot antenna array for 5G millimeter-wave massive MIMO systems," *IEEE Transactions on Antennas and Propagation*, Vol. 65, No. 12, 6721–6727, Dec. 2017.

[2] Alieldin, A., Y. Huang, S. J. Boyes, M. Stanley, S. D. Joseph, Q. Hua, and D. Lei, "A triple-band dual-polarized indoor base station antenna for 2G, 3G, 4G and sub-6 GHz 5G applications,"

[3] Hua, Q., Y. Huang, C. Song, M. O. Akinsolu, B. Liu, T. Jia, Q. Xu, and A. Alieldin, "A novel compact quadruple-band indoor base station antenna for 2G/3G/4G/5G systems," *IEEE Access*, Vol. 7, 151 350–151 358, 2019.

[4] Molins-Benlliure, J., E. Antonino-Daviu, M. Cabedo-Fabrés, and M. Ferrando-Bataller, "Four-port wide-band cavity-backed antenna with isolating X-shaped block for sub-6 GHz 5G indoor base stations," *IEEE Access*, Vol. 9, 80 535–80 545, 2021.

[5] Wen, S. and Y. Dong, "A low-profile wideband antenna with monopole-like radiation characteristics for 4G/5G indoor micro base station application," *IEEE Antennas and Wireless Propagation Letters*, Vol. 19, No. 12, 2305–2309, Dec. 2020.

[6] Lau, K. L. and K. M. Luk, "A wide-band monopolar wire-patch antenna for indoor base station applications," *IEEE Antennas and Wireless Propagation Letters*, Vol. 4, 155–157, 2005.

[7] Zhang, Z.-Y., G. Fu, W.-J. Wu, J. Lei, and S.-X. Gong, "A wideband dual-sleeve monopole antenna for indoor base station application," *IEEE Antennas and Wireless Propagation Letters*, Vol. 10, 45–48, 2011.

[8] Fu, S., X. Zhao, C. Li, and Z. Wang, "A low-profile dual-band dual-polarized dipole antenna for 5G communication applications," *Progress In Electromagnetics Research Letters*, Vol. 104, 131–137, 2022.

[9] Wen, S., Y. Xu, and Y. Dong, "A low-profile dual-polarized omnidirectional antenna for LTE base station applications," *IEEE Transactions on Antennas and Propagation*, Vol. 69, No. 9, 5974–5979, Sep. 2021.

[10] Peng, J. D., Q. D. Liu, L. H. Ye, X.-X. Tian, J.-F. Li, D.-L. Wu, and X. Y. Zhang, "Low-profile ultra-wideband dual-polarized omnidirectional antenna for indoor base station," *IEEE Transactions on Antennas and Propagation*, Vol. 71, No. 9, 7597–7602,

IEEE Access, Vol. 6, 49 209–49 216, 2018.

Sep. 2023.

[11] Dietrich, C. B., W. L. Stutzman, B.-K. Kim, and K. Dietze, "Smart antennas in wireless communications: Base-station diversity and handset beamforming," *IEEE Antennas and Propagation Magazine*, Vol. 42, No. 5, 142–151, Oct. 2000.

[12] Fan, H., X. Liang, J. Geng, R. Jin, and X. Zhou, "Switched multibeam circular array with a reconfigurable network," *IEEE Transactions on Antennas and Propagation*, Vol. 64, No. 7, 3228–3233, Jul. 2016.

[13] Ge, L., M. Li, Y. Li, H. Wong, and K.-M. Luk, "Linearly polarized and circularly polarized wideband dipole antennas with reconfigurable beam direction," *IEEE Transactions on Antennas and Propagation*, Vol. 66, No. 4, 1747–1755, Apr. 2018.

[14] Alam, M. S. and A. Abbosh, "Planar pattern reconfigurable antenna with eight switchable beams for WiMax and WLAN applications," *IET Microwaves, Antennas & Propagation*, Vol. 10, No. 10, 1030–1035, Jul. 2016.

[15] Jin, G., M. Li, D. Liu, and G. Zeng, "A simple planar pattern-reconfigurable antenna based on arc dipoles," *IEEE Antennas and Wireless Propagation Letters*, Vol. 17, No. 9, 1664–1668, Sep. 2018.

[16] Wang, P.-Y., T. Jin, F.-Y. Meng, Y.-L. Lyu, D. Erni, Q. Wu, and L. Zhu, "Beam switching antenna based on a reconfigurable cascaded feeding network," *IEEE Transactions on Antennas and Propagation*, Vol. 66, No. 2, 627–635, Feb. 2018.

[17] Kahar, M. and M. K. Mandal, "A wideband tightly coupled slot antenna for 360° full azimuthal beam steering applications," *IEEE Transactions on Antennas and Propagation*, Vol. 69, No. 6, 3538–3542, Jun. 2021.

[18] Tang, M.-C., Y. Duan, Z. Wu, X. Chen, M. Li, and R. W. Ziolkowski, "Pattern reconfigurable, vertically polarized, low-profile, compact, near-field resonant parasitic antenna," *IEEE Transactions on Antennas and Propagation*, Vol. 67, No. 3, 1467–1475, Mar. 2019.

[19] Alieldin, A., Y. Huang, S. J. Boyes, and M. Stanley, "A reconfigurable broadband dual-mode dual-polarized antenna for sectorial/omnidirectional mobile base stations," *Progress In Electromagnetics Research*, Vol. 163, 1–13, 2018.

[20] Wen, Y., P.-Y. Qin, G.-M. Wei, and R. W. Ziolkowski, "Circular array of endfire Yagi-Uda monopoles with a full 360° azimuthal beam scanning," *IEEE Transactions on Antennas and Propagation*, Vol. 70, No. 7, 6042–6047, Jul. 2022.

[21] Lu, J., D. Ireland, and R. Schlub, "Dielectric embedded ESPAR (DE-ESPAR) antenna array for wireless communications," *IEEE Transactions on Antennas and Propagation*, Vol. 53, No. 8, 2437–2443, Aug. 2005.

[22] Liu, H., S. Gao, and T. H. Loh, "Compact dual-band antenna with electronic beam-steering and beamforming capability," *IEEE*

Antennas and Wireless Propagation Letters, Vol. 10, 1349–1352, 2011.

[23] Liu, H.-T., S. Gao, and T.-H. Loh, "Electrically small and low cost smart antenna for wireless communication," *IEEE Transactions on Antennas and Propagation*, Vol. 60, No. 3, 1540–1549, Mar. 2012.

[24] Juan, Y., W. Che, W. Yang, and Z. N. Chen, "Compact pattern-reconfigurable monopole antenna using parasitic strips," *IEEE Antennas and Wireless Propagation Letters*, Vol. 16, 557–560, 2016.

[25] Wang, S.-Y., K.-X. Zhang, F. Wang, and G.-Y. Wen, "Design of a 360° continuously scanning circular array anttena," *Acta Physica Sinica*, Vol. 71, No. 24, 248402 2022.

[26] Vaskelainen, L. I., "Constrained least-squares optimization in conformal array antenna synthesis," *IEEE Transactions on Antennas and Propagation*, Vol. 55, No. 3, 859–867, Mar. 2007.

[27] Guo, J.-L. and J.-Y. Li, "Pattern synthesis of conformal array antenna in the presence of platform using differential evolution algorithm," *IEEE Transactions on Antennas and Propagation*, Vol. 57, No. 9, 2615–2621, Sep. 2009.

[28] Bai, Y.-Y., S. Xiao, C. Liu, and B.-Z. Wang, "A hybrid IWO/PSO algorithm for pattern synthesis of conformal phased arrays," *IEEE Transactions on Antennas and Propagation*, Vol. 61, No. 4, 2328–2332, Apr. 2013.

[29] Cao, K., C. Jin, B. Zhang, Q. Lv, and F. Lu, "Beam stabilization of deformed conformal array antenna based on physical-method-driven deep learning," *IEEE Transactions on Antennas and Propagation*, Vol. 71, No. 5, 4115–4127, May 2023.

[30] Morabito, A. F., A. R. Lagana, and T. Isernia, "On the optimal synthesis of ring symmetric shaped patterns by means of uniformly spaced planar arrays," *Progress In Electromagnetics Research B*, Vol. 20, 33–48, 2010.

[31] Wan, W., W. Geyi, and S. Gao, "Optimum design of low-cost dual-mode beam-steerable arrays for customer-premises equipment applications," *IEEE Access*, Vol. 6, 16 092–16 098, 2018.

[32] Miao, X., W. Wan, Z. Duan, and W. Geyi, "Design of dual-mode arc-shaped dipole arrays for indoor base-station applications," *IEEE Antennas and Wireless Propagation Letters*, Vol. 18, No. 4, 752–756, Apr. 2019.

[33] Yang, F., X.-X. Zhang, X. Ye, and Y. Rahmat-Samii, "Wideband e-shaped patch antennas for wireless communications," *IEEE Transactions on Antennas and Propagation*, Vol. 49, No. 7, 1094–1100, Jul. 2001.

[34] Geyi, W., "The method of maximum power transmission efficiency for the design of antenna arrays," *IEEE Open Journal of Antennas and Propagation*, Vol. 2, 412–430, 2021.